Progress In Electromagnetics Research M, Vol. 40, 179–193, 2014

Electromagnetic Modeling of Coupled Carbon Nanotube Dipole Antennas Based on Integral Equations System

Mourad Aidi* **and Taoufik Aguili**

Abstract—Fundamental properties of carbon nanotube antenna are firstly investigated to predict the antenna bundle response. The carbon nanotube effects are mathematically introduced via a quantum mechanical conductivity. This paper presents a new formulation based on integral equations system to study the coupled carbon nanotube antennas. The proposed integral equations system is numerically solved by the moments method. Each dipole antenna is excited at its center by a gap voltage source. The aim of the developed method is to investigate the antennas interaction effects for any coupling distance. The obtained input impedances, the current distributions and the antenna radiation patterns are in agreement with those obtained by the effective conductivity method or by the array factor method, according to the coupling distances.

1. INTRODUCTION

Carbon nanotubes (CNT) are considered as one of the carbon's allotropes, formed by a rolled-up sheet of graphene. They were discovered by Ijima in 1991 [1]. There are two kinds of CNT; Single Walled Carbon Nanotubes (SWCNT) and Multiwalled Carbon Nanotubes (MWCNT), depending on graphene's rolled-up sheet number [2]. We focus here on SWCNT. Because the crystal structure of SWCNT is strongly related to that of graphene, the tubes are typically identified using graphene's lattice vectors [3].

Depending on the structural orientation of SWCNT, determined by the lattice bases vector, there's three groups: armchair, zigzag or chiral SWCNT. Electrical and mechanical properties are strongly related to the SWCNT structural orientation: armchair SWCNT present a metallic behavior, while zigzag and chiral SWCNT can exhibit both metallic or semiconducting properties. MWCNT all exhibit metallic behavior [3].

In previous modeling works [4], CNT was considered as an antenna, but its potential performances have never been discussed. Recently, SWCNTs are synthesized with a length near to the microwave in free space, and by the way, this motivation leads to explore their properties as antenna. From other side, CNT can has metallic properties and may grow until have a length in centimeter order. In the range of centimeter and millimeter applications, CNT antennas are originally proposed by Burke [5].

In [5], CNT dipole antennas are modeled using a transmission line approach, so the following transmission line parameters; kinetic inductance $\mathbf{L}_K$, quantum capacitance $\mathbf{C}_Q$ and quantum resistance R are determined using the electrons fluid model.

Another common approach is to simulate electromagnetic wave propagation along CNT based on these electrodynamics properties [6]. This approach presents a macroscopic view for interactions of high frequency electromagnetic field with CNTs. However, the radiation efficiency of CNT antenna is very low, as a result of the slow wave surface which decreases the radiation resistance [7]. On the other hand, if we use a single CNT as dipole antenna, the problem of impedance mismatch is strongly posed. In fact, the characteristic impedance of the CNT antenna (10–100 kΩ) is greater than each of the feeding line (50 Ω). Consequently, the bundle of CNT has been proposed to solve this problem [7].

Received 14 November 2014, Accepted 30 December 2014, Scheduled 13 January 2015
* Corresponding author: Mourad Aidi (aidimourad.07@gmail.com).
The authors are with the SysCom Laboratory, National Engineering School of Tunis, BP 37 Le Belvedere 1002, Tunis, Tunisia.

In previous works CNT antennas bundle is studied based on effective axial surface conductivity for low coupling distances [8, 9]. In terahertz and infrared frequency range, the radiation characteristics of CNT dipole antenna arrays have been investigated by CST MICROWAVE STUDIO. It was shown that, $N \times N$ antenna arrays have a higher radiation efficiency than single CNT dipole antenna [10, 11]. For the CNT antennas array without coupling, the array factor approach is used to investigate the antenna radiation pattern. In this paper, some fundamental properties of finite length coupled CNT dipole antennas are rigorously described using a proposed system of N coupled integral equations. The input impedances, current distributions and the radiation antenna patterns are presented and discussed for different coupling distances. For validity purpose, obtained results are compared to those obtained by the array factor method or effective conductivity method according to the coupling distance. This paper is organized as following: in Section 2 we are interested in studying the performance of a single CNT dipole antenna. A comparison has been made to a conventional thin wire antenna of same size and shape. Section 3 presents an electromagnetic formulation based on a system of N integral equations to accurately describe the CNT dipole antenna coupling. The proposed formulation has been applied for two identical coupled CNT dipole antennas. In Section 4, we conclude this work.

2. CURRENT DISTRIBUTION FOR CNT DIPOLE ANTENNA

In this section, we are interested to investigate and discuss the CNT dipole antenna properties. In this purpose, dipole antenna is modeled as a finite cylinder excited at its center by a gap-slice with unit voltage. Figure 1 shows the antenna structure, where L and a are the antenna length and radius respectively.

2.1. Dynamic Conductivity and Integral Equation for CNT Dipole Antenna

Dynamic conductivity of CNT represents a macroscopic quantity relating to the flow electron perturbation along the CNT, due to the temporal variation of the applied electric field along it [12]. Dynamic conductivity of CNT may be calculated using the Boltzmann kinetic equation. For a small radius of CNT, the dynamic conductivity can be expressed as [6, 13]:

$$\sigma_{cn}(w) = \sigma_{zz}(w) \simeq -j\frac{2e^2 v_F}{\pi^2 \hbar a(w - j\nu)} \tag{1}$$

where $\mathbf{e}$ is the electron charge value, $\boldsymbol{\nu}$ is the relaxation electron frequency for CNT (equal to $3.10^{-12}\,\mathrm{s}^{-1}$), a is the CNT radius, $\hbar$ the reduced Planck constant and here we use the Fermi velocity as $v_F = 9,71.10^5\,\mathrm{m/s}$.

Figure 2 shows the dynamic conductivity variation as a function of frequency for different radius values of CNT. The dynamic conductivity increases when the radius decreases which shows the important conductivity of CNT with small radius.

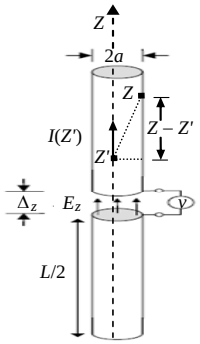

Figure 1. CNT model of cylindrical antenna.

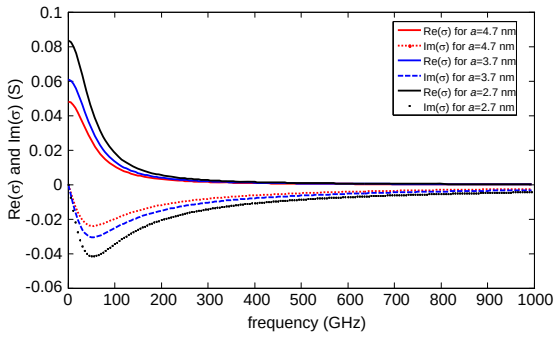

Figure 2. Dynamic conductivity as a function of frequency for different CNT radius values.

This equivalent surface conductivity is characterized by a complex value with a negative imaginary part. This latter one part represents an inductive effect that introduces a deceleration in the electromagnetic wave velocity along the CNT, which leads to reduce the wavelength. This property is so important in the passive RF devices and antennas.

CNT antenna is modeled as a finite conductive cylinder excited at its center by a slice-gap source of unit voltage. We use the dynamic conductivity to include the electrical properties of the CNT in the mathematic formulation. Then, the surface impedance per unit length of a SWCNT can be determined as:

$$Z_s = \frac{1}{2\pi a\sigma_{cn}(w)} = \frac{\pi\hbar v}{4e^2 v_F} + j\frac{\pi\hbar}{4e^2 v_F}w = R_Q + jL_K w \tag{2}$$

This electromagnetic formulation may be presented in different forms, as well as finite elements, finite difference or as an integral equation. However, electric field integral equation is the appropriate method, for a simple wire antenna.

In the case of simple CNT dipole antenna oriented along the z axis which is shown in Figure 1, the electric field at the surface of the antenna may be written as:

$$E^{in} + E^r - Z_s I = 0 \tag{3}$$

E^r is the radiated electrical field given by [6]:

$$E_z^r = \frac{1}{j4\pi w\varepsilon}\left(k^2 + \frac{\partial^2}{\partial z^2}\right)\int_{-L/2}^{L/2}\frac{e^{-jk\sqrt{(z-z')^2+a^2}}}{\sqrt{(z-z')^2+a^2}}I(z')dz' \tag{4}$$

where L is the antenna length and a is the antenna radius which will be in the order of nanometer.

By substituting the radiated electrical field expression, we have the Pocklington integral equation:

$$\left(k^2 + \frac{\partial^2}{\partial z^2}\right)\int_{-L/2}^{L/2}\frac{e^{-jk\sqrt{(z-z')^2+a^2}}}{\sqrt{(z-z')^2+a^2}}I\left(z'\right)dz' = j4\pi w\varepsilon\left(Z_s I(z) - E_z^{in}(z)\right) \tag{5}$$

Finally, we can convert the integral Equation (5) into a Hallen's integral equation, by writing [6]:

$$\left(k^2 + \frac{\partial^2}{\partial z^2}\right)\int_{-L/2}^{L/2}F\left(z-z'\right)I\left(z'\right)dz' = -j4\pi w\varepsilon E_z^{in}(z) \tag{6}$$

where the function F is given by [6]:

$$F\left(z-z'\right) = \frac{e^{-jk\sqrt{(z-z')^2+a^2}}}{\sqrt{(z-z')^2+a^2}} + \frac{w\varepsilon}{a\sigma}\frac{e^{-jk|z-z'|}}{k} \tag{7}$$

This integral equation is numerically solved using the MoM method. The antenna is divided into $N = 2M+1$ segments of length $\Delta = \frac{L}{N}$, and Equation (6) is evaluated used the delta function basis for the small sample of antenna as:

$$\left(k^2 + \frac{\partial^2}{\partial z^2}\right)V\left(z_n\right) = 2kE_z^{in}\left(z_n\right) \tag{8}$$

where:

$$V\left(z_n\right) = \frac{j\eta}{2\pi}\int_{-L/2}^{L/2}F\left(z_n - z'\right)I\left(z'\right)dz' \tag{9}$$

And η is the characteristic impedance of free space, that is expressed by: $\eta = \sqrt{\frac{\mu}{\varepsilon}}$.

We applied the finite difference approximation to the second derivative in z, which allows to rewrite Equation (8) as following:

$$k^2 V_n + \frac{V_{n+1} - 2V_n + V_{n-1}}{\Delta^2} = 2kE_n^{in} \tag{10}$$

We denote that: $V(z_n) = V_n$ and $E^{in}(z_n) = E_n^{in}$.

Then we have:

$$V_{n+1} - 2\alpha V_n + V_{n+1} = \gamma E_n \tag{11}$$

where: $\alpha = 1 - \frac{k^2\Delta^2}{2}$; $\gamma = 2k\Delta^2$ and $-(M-1) \leq n \leq M-1$.

We can convert (11) in the corresponding matrix equation, as it's shown in the matrix below for $M = 3$.

$$\begin{bmatrix} 0 & 0 & 0 & 0 & 0 & 0 & 0 \\ 1 & -2\alpha & 1 & 0 & 0 & 0 & 0 \\ 0 & 1 & -2\alpha & 1 & 0 & 0 & 0 \\ 0 & 0 & 1 & -2\alpha & 1 & 0 & 0 \\ 0 & 0 & 0 & 1 & -2\alpha & 1 & 0 \\ 0 & 0 & 0 & 0 & 1 & -2\alpha & 1 \\ 0 & 0 & 0 & 0 & 0 & 0 & 0 \end{bmatrix} \begin{bmatrix} V_{-3} \\ V_{-2} \\ V_{-1} \\ V_0 \\ V_1 \\ V_2 \\ V_3 \end{bmatrix} = \gamma \cdot \begin{bmatrix} 0 & 0 & 0 & 0 & 0 & 0 & 0 \\ 0 & 1 & 0 & 0 & 0 & 0 & 0 \\ 0 & 0 & 1 & 0 & 0 & 0 & 0 \\ 0 & 0 & 0 & 1 & 0 & 0 & 0 \\ 0 & 0 & 0 & 0 & 1 & 0 & 0 \\ 0 & 0 & 0 & 0 & 0 & 1 & 0 \\ 0 & 0 & 0 & 0 & 0 & 0 & 0 \end{bmatrix} \begin{bmatrix} E_{-3} \\ E_{-2} \\ E_{-1} \\ E_0 \\ E_1 \\ E_2 \\ E_3 \end{bmatrix} \tag{12}$$

We can write (12) as: $AV = \gamma\delta E$ where δ is the projection matrix. We note that P is its complement $P = I_d - \delta$, which enforce the edges conditions ($I_{\pm M} = 0$).

$$PI = (I_d - \delta)\, I = 0 \tag{13}$$

The current distribution along the CNT is expressed as the sum of the samples current I_m using a basis function $B(z)$:

$$I(z) = \sum_{m=-M}^{M} I_m B(z - z_m) \tag{14}$$

Then Equation (9) is rewritten as following:

$$V(z_n) = \sum_{m=-M}^{M} I_m \frac{j\eta}{2\pi} \int_{-L/2}^{L/2} F\left(z_n - z'\right) B\left(z'\right) dz = \sum_{m=-M}^{M} Z_{nm} I_m \tag{15}$$

So the impedance matrix is given by:

$$Z_{nm} = \frac{j\eta}{2\pi} \int_{-L/2}^{L/2} F\left(z_n - z'\right) B\left(z'\right) dz \tag{16}$$

Therefore, we deduce the current vector as: $I = \delta A^{-1} Z^{-1} \delta E$.

Using the current distribution found by MoM method, we compute the input impedance as: $Z_{in} = \frac{U_0}{I_0}$.

The current distribution in the CNT antenna can be considered in one dimension, and its time variation will generate a radiated electrical far field in the surrounding free space [4]:

$$E_\theta = i\eta \frac{k e^{-jkr}}{4\pi r} \sin\theta \left[\int_{-L/2}^{L/2} I(z) e^{jkz\cos\theta} dz \right] \tag{17}$$

where η is the free space characteristic impedance, L and r are respectively the dipole length and radius, and θ is the elevation angle coordinate.

2.2. Numerical Results of Single CNT Dipole Antenna

In this section, we give a quantitative discussion concerning the single CNT dipole antenna response to a delta gap source of unit voltage localized in its center. Firstly we are interested to study the convergence of our problem. Figure 3(a) presents the input impedance variation in function of the segments number N, for different used basis function. Like in the delta-gap case, the triangular and pulse basis functions converge the faster. For large values of N, all the bases functions produces the same results with the exception of the delta basis function which converges very slowly. To illustrate the convergence properties, the current distribution of the half length wave CNT antenna is represented in Figure 3(b) using a pulse basis function for different values of N. This result is in agreement with

that found using input impedance. For the rest of paper, we used the pulse as a basis function and the segments number is fixed to $N = 2M + 1 = 100$ to ensure convergence.

Figure 4(a) and Figure 4(b) present the complex input impedance of CNT antenna and perfectly conducting thin wire antenna of same size and shape, as a function of the frequency. The length of the dipole antenna is $L = 20\,\mu\text{m}$, and the radius is assumed to 2.71 nm. It can be noted that, the CNT antenna has a first resonance nearly to 150 GHz yielding a propagation velocity $v_p = 0.01c$, where c is the light velocity in the vacuum. However, the perfectly conducting thin wire antenna does not has any resonance at this frequency range. The first resonance appears nearly at 7500 GHz yielding a propagation velocity $v = 0.5c$. Therefore, the resonant frequencies corresponding to a velocity reduction factor in the order of 0.02. This reduction is due to the excess of kinetic inductance in the CNT. This kinetic induction has much greater value compared to the conventional magnetic inductance of perfectly conducting thin wire antenna [4]. The excess inductance has a significant effect on slowing the electromagnetic propagation velocity along CNT, which leads to reduce the wavelength.

We present the radiation pattern of the CNT dipole antenna and conventional thin wire antenna for lengths $L = 20\,\mu\text{m}$ and $L = 2\,\text{mm}$ respectively. The operating frequency is around $f = 150\,\text{GHz}$. Obtained results were illustrated in Figure 5(a). Note that the conventional thin wire antenna is more directive than the CNT antenna. If the length of the conventional thin wire antenna is in the order of 0.01λ, the two antennas generates the same radiation pattern. Therefore, the CNT antenna wavelength noted λ_p should be approximately 100 times smaller than the free space wavelength ($\lambda_p \approx 0.01\lambda$), where λ_p is called plasmon wavelength [4].

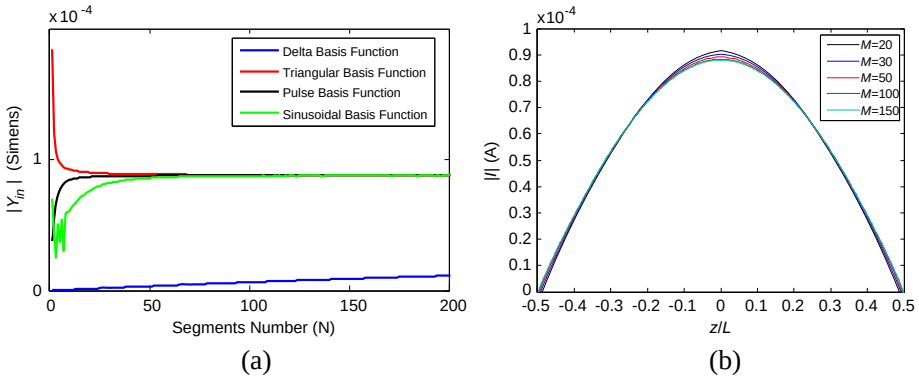

Figure 3. (a) Input Impedance as a function of number of segments for different basis functions. (b) Current distribution as a function of the basis function number. This results are obtained for antenna length $L = 20\,\mu\text{m}$, radius $a = 2.71\,\text{nm}$ and operating frequency $f = 150\,\text{GHz}$.

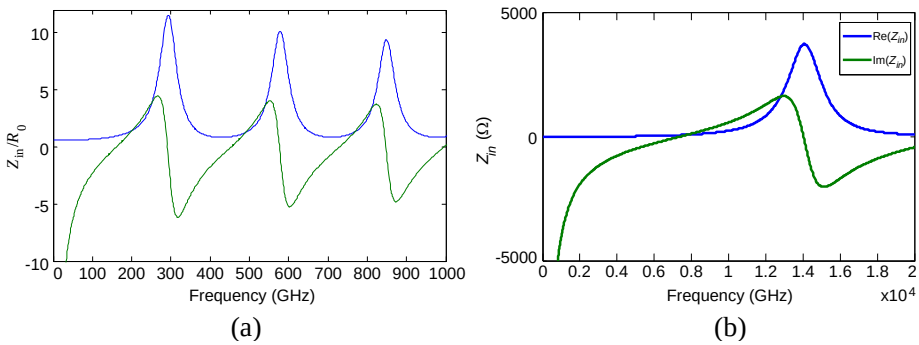

Figure 4. (a) Input impedance as a function of the frequency for CNT antenna of length $L = 20\,\mu\text{m}$ and radius $a = 2.71\,\text{nm}$, $R_0 = 12.9\,\text{k}\Omega$. (b) Input impedance as a function of the frequency for perfectly conducting thin wire antenna of the same size and shape.

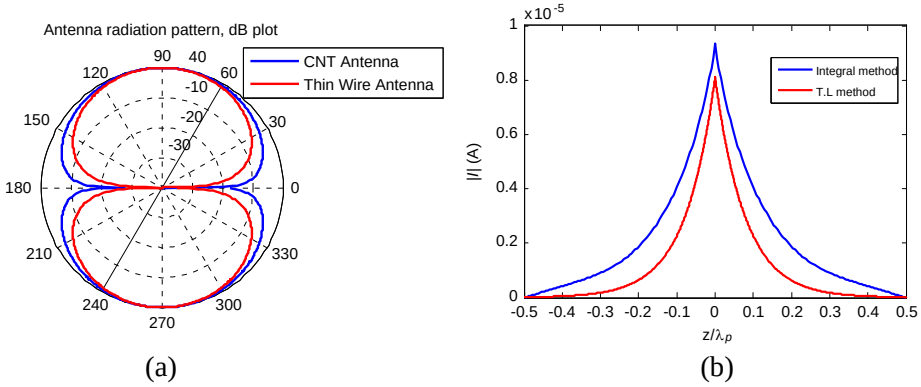

Figure 5. (a) Antenna radiation pattern obtained on a CNT dipole antenna and perfectly conducting thin wire antenna of length $L = 20\,\mu\text{m}$ and $L = 2\,\text{mm}$ respectively, for operating frequency $f = 150\,\text{GHz}$. (b) Current distribution on a CNT dipole antenna using MoM method and transmission line method for an antenna length $L = 300\,\mu\text{m}$ and operating frequency $f = 10\,\text{GHz}$.

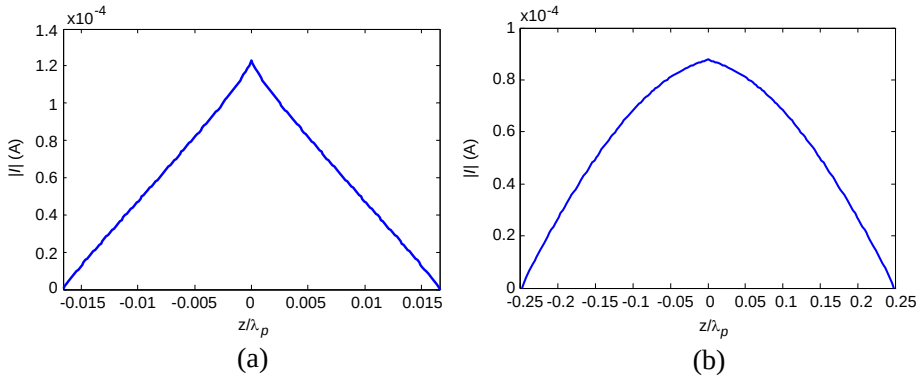

Figure 6. Current distribution obtained on a CNT dipole antenna of length $L = 20\,\mu\text{m}$ and radius $a = 2.71\,\text{nm}$. (a) Operating frequency $f = 10\,\text{GHz}$. (b) Operating frequency $f = 150\,\text{GHz}$.

As it is shown in Figure 5(b), MoM method and transmission line method gives nearly the same current distribution for a CNT dipole antenna of length $300\,\mu\text{m}$ for operating frequency $10\,\text{GHz}$.

For an operating frequency insufficient to reach the first resonance, the current distribution take approximately a triangular form, like the ordinary short dipole which is shown in Figure 6(a). For operating frequency around the first resonance, the current distribution is shown in Figure 6(b). In this case, the current distribution is approximately a half sinusoid for operating frequency $f = 150\,\text{GHz}$ and antenna length $L = 20\,\mu\text{m}$ which corresponds to $L = \lambda_p/2$. It can also be noted that, the CNT antenna length is nearly 0.01 times the length of the ordinary half-wave length antenna at this frequency, which gives a scaling reduction factor of nearly 0.01 ($\lambda_p = 0.01\lambda$). This results represents an important miniaturization of antennas structures which makes the CNT antenna a good candidate for microwave applications. If the frequency is doubled, the current distribution is a sinusoid which is corresponding to an antenna with a length equal to λ_p.

The current intensity at the center of CNT dipole antenna is plotted versus the antenna radius in Figure 7 (a). The antenna is excited at the center by a unit delta-gap source for an operating frequency $f = 150\,\text{GHz}$. This result proves that the variation of the antenna radius affects only the magnitude of current distribution. In Figure 7(b), we can see that the changes in the CNT antenna radius does not affect the current distribution shape. It remains approximately a half-sinusoid, which corresponds to a current distribution of half wavelength antenna ($L = \lambda_p/2$). If we decrease progressively the antenna radius there is a proportional current peak that appears in the antenna center reflecting the source effect.

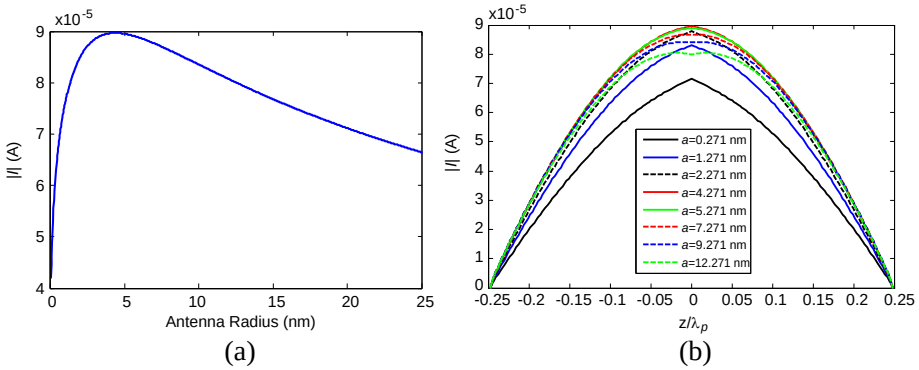

Figure 7. (a) Current intensity at the antenna center as a function of antenna radius values. (b) Current distribution on a CNT antennas of same lengths $L = 20\,\mu\text{m}$ and different radius values for operating frequency $f = 150\,\text{GHz}$.

3. COUPLED CARBON NANOTUBE DIPOLE ANTENNAS

The mutual coupling phenomenon between antennas cannot be neglected if the antennas are near each other. The mutual impedance is a measure of the interaction effects between the near antennas [14, 15].

3.1. Integral Equations for N Coupled CNT Dipole Antennas

Consider N identical parallel CNT dipole antennas center-driven by the generators $V_1, V_2, \ldots, V_N$. Their centers are separated by the distance d along the x-direction. $I_1(z), I_2(z), \ldots, I_N(z)$ are the currents on the CNT dipoles antennas induced by the generators and the mutual interactions. The antennas have the same length and radius. The antenna radius is very small compared to the antenna length, then the total current density will has only the z-component given by [16, 17]:

$$J_z\left(x', y', z'\right) = \sum_{p=1}^{N} I_p\left(z'\right)\delta\left(x' - x_p\right)\delta\left(y' - y_p\right) \tag{18}$$

Taken into account the form of the total current density, the z-component of the scattered electric field generated by the currents will be:

$$E_z(z) = \frac{1}{j4\pi w\varepsilon\mu}\sum_{p=1}^{N}\left(\frac{\partial^2}{\partial z^2} + k^2\right)\int_{-\frac{L}{2}}^{\frac{L}{2}}\frac{e^{-jkR_p}}{R_p}I_p(z')dz' \tag{19}$$

where R_p is the distance from the observation point (x, y, z) to the z' point on the each antenna.

Thus, on the surfaces of each antenna we write:

$$\begin{cases} E_{11}^d + E_{21}^d + E_{31}^d + \ldots + E_{N1}^d - Z_s I_1 = -E_1^{in} \\ E_{12}^d + E_{22}^d + E_{32}^d + \ldots + E_{N2}^d - Z_s I_2 = -E_2^{in} \\ \vdots \\ E_{1N}^d + E_{2N}^d + E_{3N}^d + \ldots + E_{NN}^d - Z_s I_N = -E_N^{in} \end{cases} \tag{20}$$

where E_{pq} is the z-component of the electric field on the antenna p induced by the current on the antenna q:

$$E_{pq}(z) = \left(\frac{\partial^2}{\partial z^2} + k^2\right)\int_{-\frac{l}{2}}^{\frac{l}{2}}\frac{e^{-jkR_{pq}}}{R_{pq}}I_q\left(z'\right)dz' = \widehat{G}_{pq}I_q \tag{21}$$

Knowing that:

$$\widehat{G}_{pq} = \frac{1}{j4\pi w\varepsilon}\left(k^2 + \frac{\partial^2}{\partial z^2}\right)\int_{-h}^{h}\frac{e^{-jkR_{pq}}}{R_{pq}}dz' \tag{22}$$

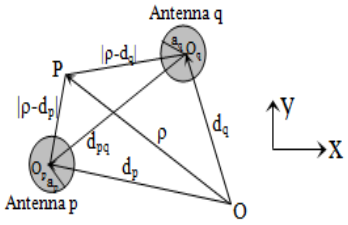

Figure 8. Array of linear dipole antennas.

and

$$R_{pq} = \sqrt{(z - z')^2 + d_{pq}^2} \tag{23}$$

That is shown in Figure 8, d_{pq} is the coupling distance which is calculated as follows [14, 18]:

$$\begin{cases} d_{pq} = \sqrt{(x_p - x_q)^2 + (y_p - y_q)^2} & \text{if } p \neq q \\ d_{pq} = a_p & \text{if } p = q \end{cases} \tag{24}$$

Then we obtain a system of N integral equations:

$$\begin{cases} \widehat{G}_{11}I_1 + \widehat{G}_{21}I_1 + \widehat{G}_{31}I_1 + \ldots + \widehat{G}_{N1}I_1 - Z_sI_1 = -E_1^{in} \\ \widehat{G}_{12}I_2 + \widehat{G}_{22}I_2 + \widehat{G}_{32}I_2 + \ldots + \widehat{G}_{N2}I_2 - Z_sI_2 = -E_2^{in} \\ \vdots \\ \widehat{G}_{1N}I_N + \widehat{G}_{2N}I_N + \widehat{G}_{3N}I_N + \ldots + \widehat{G}_{NN}I_N - Z_sI_N = -E_N^{in} \end{cases} \tag{25}$$

By using a testing (weighting) function $g_n(z)$, which is centered on z_n for each antenna p, (28) can be written as:

$$\begin{cases} \left\langle g_{1n}, \left(\widehat{G}_{11} - Z_s\right) I_1 \right\rangle + \left\langle g_{1n}, \widehat{G}_{21}I_2 \right\rangle + \left\langle g_{1n}, \widehat{G}_{31}I_3 \right\rangle + \ldots + \left\langle g_{1n}, \widehat{G}_{N1}I_N \right\rangle = -\left\langle g_{1n}, E_1^{in} \right\rangle \\ \left\langle g_{2n}, \widehat{G}_{21}I_1 \right\rangle + \left\langle g_{2n}, \left(\widehat{G}_{22} - Z_s\right) I_2 \right\rangle + \left\langle g_{2n}, \widehat{G}_{32}I_3 \right\rangle + \ldots + \left\langle g_{2n}, \widehat{G}_{N3}I_N \right\rangle = -\left\langle g_{2n}, E_2^{in} \right\rangle \\ \vdots \\ \left\langle g_{Nn}, \widehat{G}_{N1}I_1 \right\rangle + \left\langle g_{Nn}, \widehat{G}_{N2}I_1 \right\rangle + \left\langle g_{Nn}, \widehat{G}_{N3}I_1 \right\rangle + \ldots + \left\langle g_{Nn}, \left(\widehat{G}_{NN} - Z_s\right) I_N \right\rangle = -\left\langle g_{Nn}, E_N^{in} \right\rangle \end{cases} \tag{26}$$

The current along the CNT is expressed as the sum of the current samples I_n using a basis functions $f(z)$:

$$I_q(z) = \sum_{m=-N}^{N} I_{qm} f(z - z_m) \tag{27}$$

Therefore, we convert this system into a matrix form and deduce the current distribution for each dipole antenna:

$$\begin{bmatrix} \left[\left\langle g_{1n}, \left(\widehat{G}_{11} - Z_s\right) f_{1m} \right\rangle\right] & \ldots & \left[\left\langle g_{1n}, \widehat{G}_{N1} f_{1m} \right\rangle\right] \\ \vdots & \ddots & \vdots \\ \left[\left\langle g_{Nn}, \widehat{G}_{1N} f_{Nm} \right\rangle\right] & \ldots & \left[\left\langle g_{nN}, \left(\widehat{G}_{NN} - Z_s\right) f_{Nm} \right\rangle\right] \end{bmatrix} \begin{bmatrix} I_1 \\ \vdots \\ I_N \end{bmatrix} = - \begin{bmatrix} \left[\left\langle g_{1n}, E_1^{in} \right\rangle\right] \\ \vdots \\ \left[\left\langle g_{Nn}, E_N^{in} \right\rangle\right] \end{bmatrix} \tag{28}$$

3.2. Integral Equation Based on Equivalent Dynamic Conductivity for N Coupled CNT Dipole Antennas

In the case of very small inter-tubes distances, the array elements are strongly coupled, and the medium is considered as a single antenna with effective surface conductivity σ [9, 19, 20]. In the Figure 9, we

consider a densely packed bundle of single walled carbon nanotubes (SWCNT) having a circular cross section with radius R and length L. The bundle is formed by N metallic SWCTs with radius a, which are connected in parallel at their centers by a delta gap source with unit voltage.

The effective surface conductivity of the formed antenna is defined by [8]:

$$\sigma \simeq \frac{N\sigma_{cn}(w)a}{R} \tag{29}$$

The electromagnetic wave interaction between CNT antennas is modeled by the integral equation like the analysis of the single antenna seen in first section. The basic idea is to use the integral equation as single CNT antenna based on Hallen's integral equation, with a slightly modification to include the surface conductivity of the bundle.

$$\left(k^2 + \frac{\partial^2}{\partial z^2}\right) \int_{-h}^{h} \left(\frac{e^{-jk\sqrt{(z-z')^2+a^2}}}{\sqrt{(z-z')^2+a^2}} + \frac{w\varepsilon}{a\sigma} \frac{e^{-jk|z-z'|}}{k} \right) I\left(z'\right) dz' = -j4\pi w\varepsilon E_z^{in}(z) \tag{30}$$

This integral equation can be solved numerically using the MoM method, and follows the same steps as in the case of a single antenna described in the first section. Based on the obtained current distribution, we deduce the input impedance and other antenna parameters.

3.3. Pattern Multiplication: Array Factor

The array factor $(A \cdot F)$ is function of the antenna parameters. It depends on the element number, the coupling distance, phase and amplitude of the applied signal to each element. If the antennas are isolated, we can assume that all the polar radiation patterns of the elements taken individually are identical and that the patters are all aligned in the same direction in azimuth and elevation. The total array antenna pattern is got by multiplying the array factor $(A \cdot F)$ by the element pattern.

The general form of the $A \cdot F$ for a linear array with uniform elements spacing is given by [21]:

$$A \cdot F = 1 + e^{j(kd\cos(\theta)+\delta)} + e^{2j(kd\cos(\theta)+\delta)} + \ldots + e^{j(N-1)(kd\cos(\theta)+\delta)} \tag{31}$$

where $k = \frac{2\pi}{\lambda}$, N is the elements number and δ is phase shift and θ is the elevation angle.

This section applied a one dimensional symmetric linear antenna array of N-identical elements regularly positioned along x-axis and equally positioned by a distance d, see Figure 10. The array

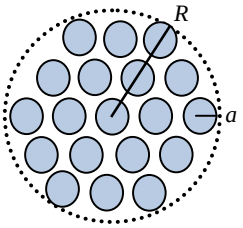

Figure 9. Schematic structure of SWCNT bundle.

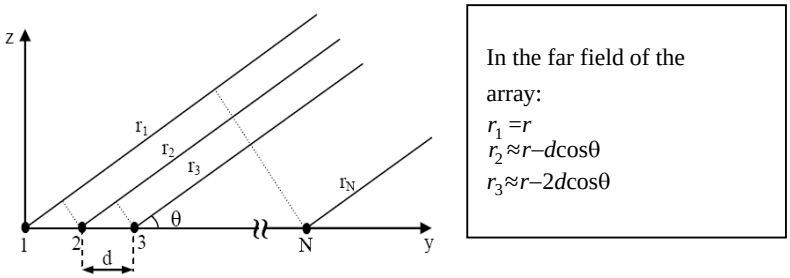

Figure 10. The linear array on the y-axis of N-elements.

factor of N elements can be written as [22]:

$$A \cdot F = \sum_{n=1}^{N} e^{j(n-1)\psi} \tag{32}$$

where $\psi = kd\cos(\theta) + \delta$ is defined as the array phase function which depending to the phase shift, the elevation angle and the elements spacing.

Finally, if the $A \cdot F$ is multiplied by $e^{j\psi}$, we come up with [23]:

$$A \cdot F = \frac{\sin\left(N\dfrac{\psi}{2}\right)}{\sin\left(\dfrac{\psi}{2}\right)} e^{j(N-1)\frac{\psi}{2}} \tag{33}$$

where $\theta \geq 0$ and $0 \leq \delta \leq 2\pi$.

Practically, in the array factor, the amplitude of the radiated fields is often important than the phase. So, we just take the norm of the array factor.

$$|A \cdot F| = \left| \frac{\sin\left(N\dfrac{\psi}{2}\right)}{\sin\left(\dfrac{\psi}{2}\right)} \right| \tag{34}$$

Also, what often matters is the relative level of the field when the direction change. Then we use a normalized array factor where its value does not exceed one.

4. NUMERICAL RESULTS

In this section, we give a quantitative discussion concerning the coupling of aligned single CNT dipole antennas. In the following, we present different numerical results for various parameters: coupling distance, CNT number and choice of used method.

Figure 11 shows the structure of the problem, we consider two parallel center-driven coupled CNT antennas with identical size and shape.

4.1. Study of Coupling Depending to the Separate Distance

We are interested in the assessment of the current distribution induced along each CNT dipoles antennas. All antennas are excited at its centers by a gap-slice source of unit voltage. Assuming that we have two identical coupled CNT antennas with lengths $L = 20\,\mu\text{m}$ and radius $a = 2.71\,\text{nm}$ for operating frequency $f = 150\,\text{GHz}$. First, we are interested in evaluating the coupling effects when the coupling distance changes.

Figure 12 presents the normalized norm of the mutual coupling matrix as a function of the coupling distance d. For a coupling distances that are much greater than the half wavelength ($d > 0.5\lambda_p$), the norm of the mutual coupling matrix vanishes like $1/d$. Indeed, there are three coupling regions:

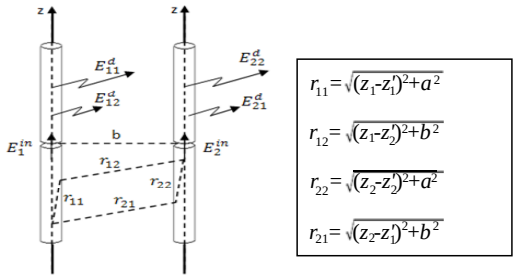

Figure 11. Array of two identical parallel linear antennas.

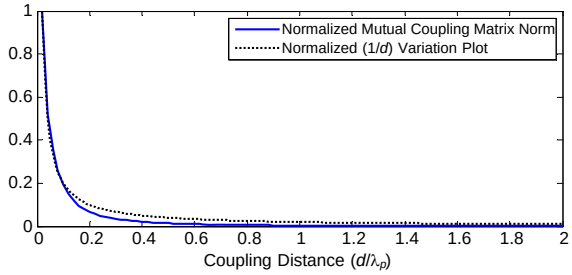

Figure 12. Normalized mutual coupling matrix norm as a function of the coupling distance. Obtained result of two identical coupled antennas with the same length $L = 20\,\mu\text{m}$ and operating frequency $f = 150\,\text{GHz}$.

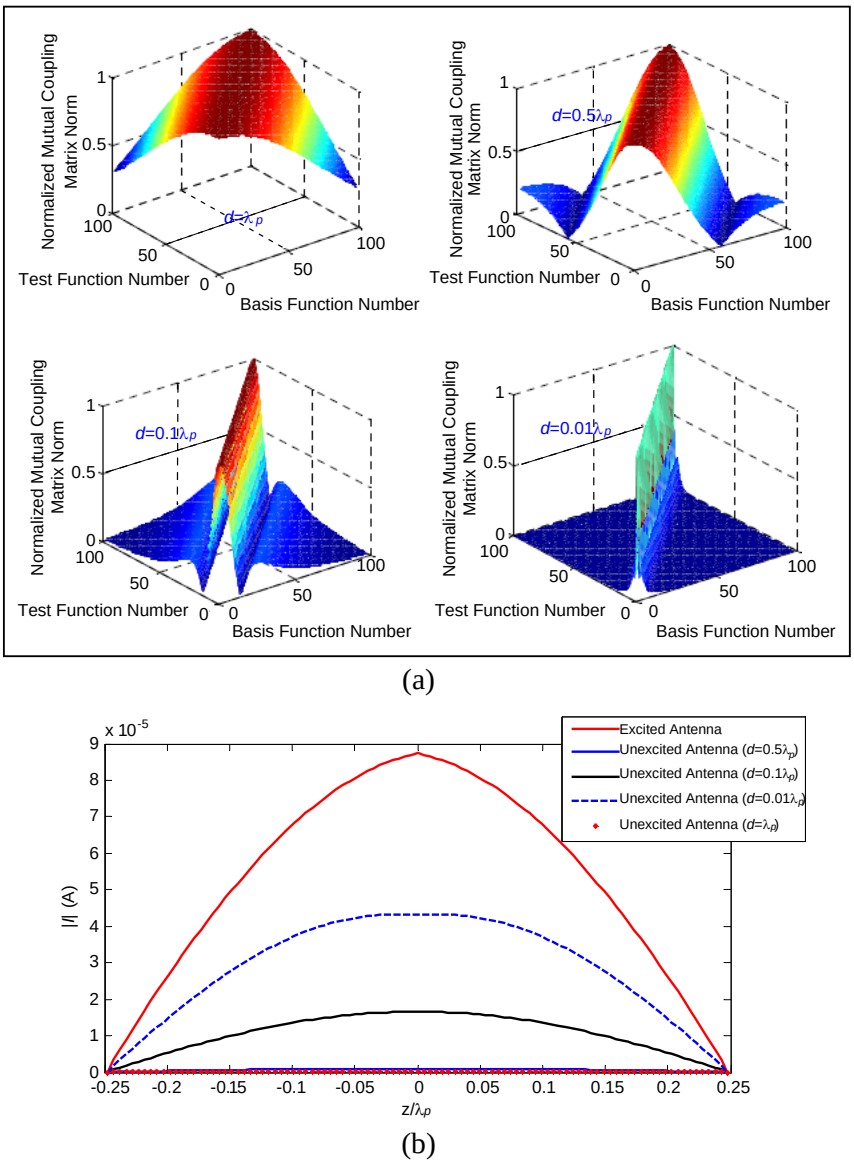

Figure 13. (a) Normalized mutual coupling matrix for different coupling distances. (b) Current distribution along each CNT dipole antennas for different coupling distances. Results obtained for coupled antennas with lengths $L = 20\,\mu\text{m}$ and radius $a = 2.71\,\text{nm}$ for operating frequency $f = 150\,\text{GHz}$.

- Strongly coupled antennas, where the coupling distance does not exceed $0.2\lambda_p$.
- Weakly coupled antennas, where the coupling distance can reach $0.75\lambda_p$.
- Isolated antenna, for a coupling distance greater than $0.75\lambda_p$.

We present in Figure 13(a) the normalized mutual coupling matrix of two coupled CNT dipole antennas for different coupling distances ($d = 0.5\lambda_p$, $d = 0.1\lambda_p$ and $d = 0.01\lambda_p$). For a coupling distance values greater than the half-length of the dipole antenna, the mutual coupling matrix takes a non diagonal form, and the coupling effects vanishes. Figure 13(b) shows that, the current distribution of the excited antenna is more greater than each of the unexcited antenna for a coupling distances $d > 0.5\lambda_p$, this confirms the weak coupling effect. In fact, the current distribution along the unexcited antenna is induced by the incident electric field radiated by the excited antenna. If the coupling distance increases, the electric field effect in the unexcited antenna decreases like $1/d$, which is confirmed by Figure 12. For a coupling distances that exceed λ_p, the current distribution vanishes and the antennas are considered as isolated. Furthermore, the current distribution of each antenna is approximately a half sinusoid for an operating frequency $f = 150\,\text{GHz}$ and antennas lengths $L = 20\,\mu\text{m}$ which corresponds to the first resonance. Likewise, for a coupling distance $d = 0.1\lambda_p$, the mutual coupling matrix takes nearly a diagonal form. In fact, the matrix elements vanish compared to each of the diagonal. Consequently, the current distribution of the unexcited antenna keeps the same shape with amplification of the magnitude.

From Figure 13, it can be noted that, when the antennas are strongly coupled ($d = 0.01\lambda_p$), they generate approximately the same current distribution, with a diagonal mutual coupling matrix.

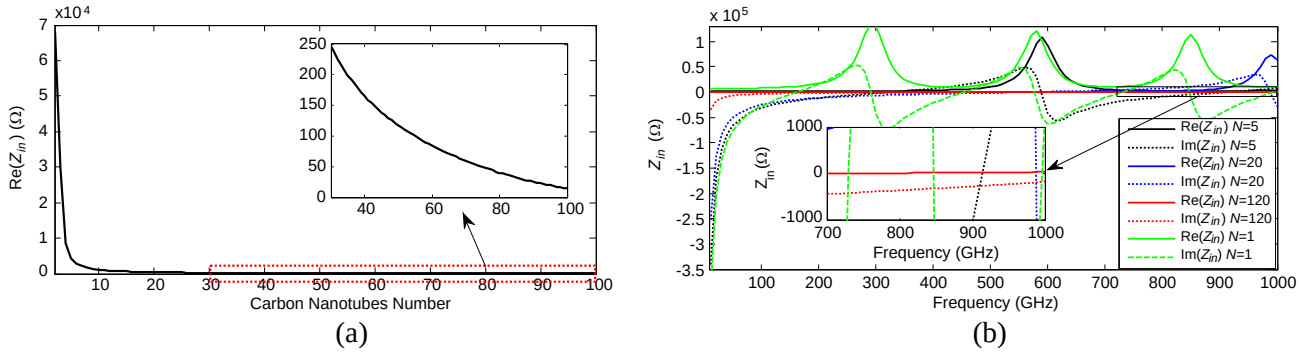

Figure 14. (a) Real part of input impedance as a function of the carbon nanotube number for operating frequency $f = 430\,\text{GHz}$. (b) Real and imaginary part of the input impedance as a function of the frequency for different number of carbon nanotube.

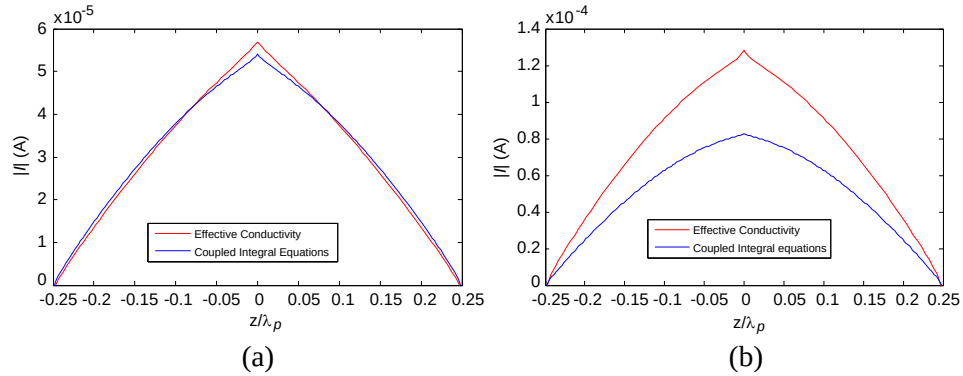

Figure 15. (a) Total current distribution for two adjacent CNT dipole antennas ($d = 0.01\lambda_p$). (b) Total current distribution for two strongly coupled CNT dipole antennas ($d = 0.2\lambda_p$). Results obtained for antenna lengths $L = 20\,\mu\text{m}$, radius $a = 2.71\,\text{nm}$ and operating frequency $f = 150\,\text{GHz}$.

4.2. CNT Number Effects

Figure 14(a) shows the real part of the input impedance as a function of the CNT number in the bundle. The length of the antenna bundle is assumed to be 20 µm at 150 GHz of frequency. It should be noted that the input impedance is monotonically decreased if the number of CNT increases. In this case, adaptation to 50 Ω is obtained for a number of carbon nanotubes $N = 75$. We represent in Figure 14(b), the input impedance for different values of N. For the case of $N = 8$, the first resonance occurs nearly at the frequency $f = 430$ GHz for a resonance impedance in the order of 1645 Ω. If we compare this results to the conventional half-wavelength dipole antenna, CNT dipole antenna has an important scale reduction factor of 0.057. For $N = 20$, the resonance frequency is nearly to $f = 600$ GHz and the resonance impedance is in the order of 687 Ω. Therefore, the scale reduction factor reaches a value of 0.08. It can be noted that the antenna bundle formed by $N = 120$ carbon nanotubes, does not resonate for this frequency range. So, for a fixed CNT length and radius, the input impedance is inversely proportional to the CNT number. If the CNT number increases, the resonance frequency shifts to the high values.

4.3. Array Antenna Radiation Pattern

As described in Figure 12, our study is focused in three regions according to the coupling intensity. As shown in Figure 15(a), if the coupling distance is very low ($d = 0.01\lambda_p$), which does not exceed $0.1\lambda_p$, obtained total current distribution will be in agreement with that obtained by effective conductivity method. Increasing the coupling distance ($d = 0.2\lambda_p$), the array elements interaction decreases gradually. It can be noted that, for the effective conductivity method, there is a shift in the resonance frequency to the lower values.

Similarly, the current amplitude moves towards higher values (Figure 15(b)). When the coupling distance increases even more, the effective conductivity method diverges due to the errors introduced by the average conductivity computation. For a comparison purpose, we determine the radiation pattern generated by the antenna array, using all methods described previously. The array is formed

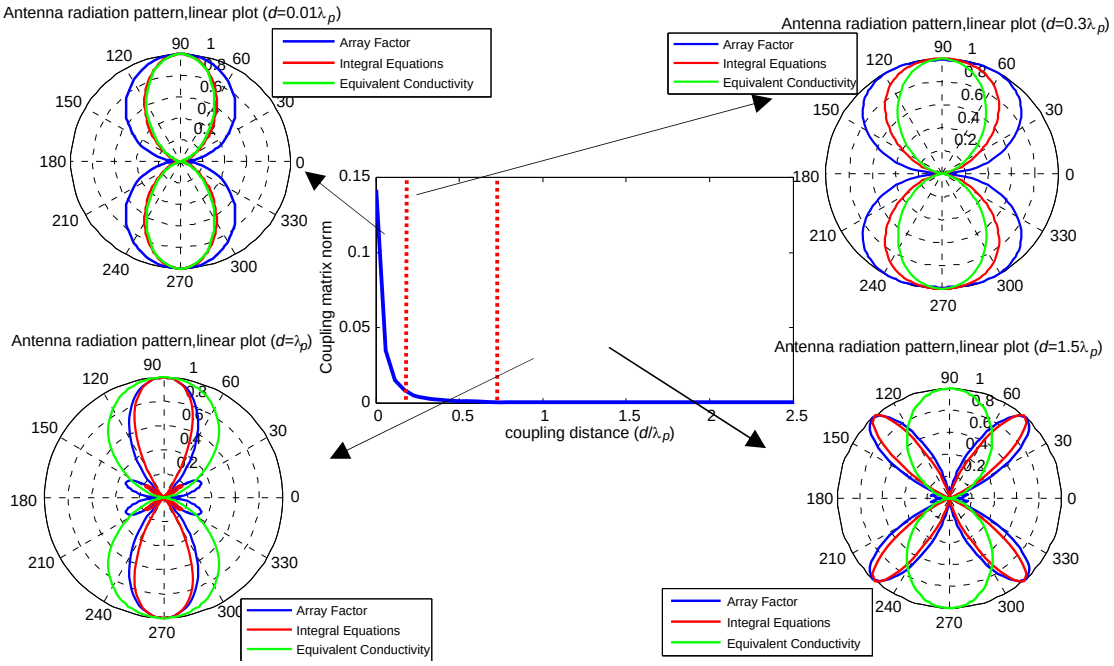

Figure 16. Array antenna radiation pattern obtained using effective conductivity approach, the proposed coupled integral equations approach and array factor method. Results obtained for different coupling distances.

by two identical antennas with length $L = 20\,\mu\text{m}$ and radius $a = 2.71\,\text{nm}$. For operating frequency $f = 150\,\text{GHz}$, obtained results are illustrated in Figure 16. We note that, for a strongly coupled antennas ($d = 0.01\lambda_p$), our proposed approach and effective conductivity method gives the same results, whereas $A \cdot F$ method behaves differently. This is explained by the fact of not isolated antennas. In fact, in the $A \cdot F$ computation we assume that all antennas produce the same radiation pattern modulus that remain constant. However, for a weakly coupling distances ($d < 0.5\lambda_p$) we cannot neglect the antenna interaction and the radiation patterns of each dipole antenna are perturbed.

For a coupling distance $0.2\lambda_p < d < 0.75\lambda_p$, results obtained by different methods are not in agreement. Increasing the coupling distance, only our proposed approach and $A \cdot F$ method are in accordance. This is shown for coupling distance $d = \lambda_p$ and $d = 1.5\lambda_p$. Consequently, we demonstrate that our approach can be accurately applied for any coupling distance.

5. CONCLUSION

In this paper, we have investigated the carbon nanotube dipole antenna properties based on Hallen's-type integral equation. The CNT effects are mathematically introduced using a rigorous quantum mechanical conductivity. A comparison has been made to a conventional thin wire antenna of same size and shape. It is found that, we cannot think of a CNT dipole antenna in the same way as a thin wire antenna. In fact, this difference is due to the excess of the inductance, approximately of 10^4 time greater than the inductance of a thin-wire antenna. Obtained results indicates that CNT dipole antenna displays similar characteristics as well as thin wire antenna, but offer an advantage of higher frequency.

Because the CNT dipole antenna presents a high input impedance, the problem of impedance mismatch is strongly posed. To solve this problem, CNT antennas array is studied and the proposed formulation based on a system of integral equations allows to accurately describe the interaction between the array elements for any coupling distance. For validation purpose, the proposed approach has been applied to a structure formed by two coupled CNT dipole antennas. Obtained results are in the agreement with those obtained by the effective conductivity approach or the array factor method according to the coupling distance. This proposed formulation can be also applied to study an irregular antenna array with any shape.

REFERENCES

1. Iijima, I., "Helical microtubules of graphitic carbon," *Nature*, Vol. 354, 56–58, 1991.
2. Saito, R., G. Dresselhaus, and M. S. Dresselhaus, *Physical Properties of Carbon Nanotubes,* Imperial College Press, London, UK, 2003.
3. Charlier, J.-C., X. Blase, and S. Roche, "Electronic and transport properties of nanotubes," *Reviews of Modern Physics*, Vol. 79, 677, Apr.–Jun. 2007.
4. Burke, P. J., "An RF circuit model for carbon nanotubes," *IEEE Trans. Nanotechnol.*, Vol. 2, No. 1, 55–58, Mar. 2003.
5. Burke, P. J., S. Li, and Z. Yu, "Quantitative theory of nanowire and nanotubes antenna performance," *IEEE Trans. Nanotechnol.*, Vol. 5, No. 4, 314–334, Jul. 2006.
6. Hanson, G. W., "Fundamental transmitting properties of carbon nanotubes antennas," *IEEE Transactions on Antennas and Propagation*, Vol. 53, No. 11, 3426–3435, Washington, DC, Jul. 2–3, 2005.
7. Plombon, J. J., K. P. O'Brien, F. Gstrein, and V. M. Dubin, "High-frequency electrical properties of individual and bundled carbon nanotubes," *Applied Physics Letters*, Vol. 90, 063106, 2007.
8. Attiya, A. M., "Lower frequency limit of carbon nanotube antenna," *Progress In Electromagnetics Research*, Vol. 94, 419–433, 2009.
9. Huang, Y., W.-Y. Yin, and Q. H. Liu, "Performance prediction of carbon nanotube bundle dipole antennas," *IEEE Trans. Nanotechnol.*, Vol. 7, No. 3, 331–337, May 2008.
10. Lan, Y., B. Zeng, H. Zhang, B. Chen, and Z. Yang, "Simulation of carbon nanotube THz antenna arrays," *International Journal of Infrared and Millimeter Waves*, Vol. 27, No. 6, 871–877, Jun. 2006.

11. Wang, Y., Q. Wu, W. Shi, X. He, X. Sun, and T. Gui, "Radiation properties of carbon nanotubes antenna at terahertz/infrared range," *International Journal of Infrared and Millimeter Waves*, Vol. 29, No. 1, 35–42, 2008.
12. Ren, L., Q. Zhang, S. Nanot, I. Kawayama, M. Tonouchi, and J. Kono, "Terahertz dynamics of quantum-confined electrons in carbon nanomaterials," *Journal of Infrared, Millimeter, and Terahertz Waves*, Vol. 33, 846–860, 2012.
13. Nefedov, I. S., "Effects of electromagnetic interaction in periodic arrays of single-wall metallic carbon nanotubes," *Materials Physics and Mechanics*, Vol. 13, 1–8, 2012.
14. Aidi, M. and T. Aguili, "Performance prediction of coupled carbon nanotubes dipole antennas," *IEEE Conference on Electromagnetic Field Computation CEFC*, May 2014.
15. Schelkunoff, S. A. and H. T. Friis, *Antennas Theory and Practice,* Wiley, New York, 1952.
16. Kelley, D. F. and W. L. Stutzman, "Array antenna pattern modeling methods that include mutual coupling effects," *IEEE Transactions on Antennas and Propagation*, Vol. 41, No. 12, 1625–1632, Dec. 1993.
17. Orfanidis, S. J., *Electromagnetic Waves and Antennas,* The MathWorks, Inc., ISBN: 0130938556.
18. Omri, D., M. Aidi, and T. Aguili, "Transient response of coupled wire antennas using the electric field integral equation with Laguerre polynomials as temporal basis functions," *IEEE International Conference on Ultra-Wideband*, 245–250, Paris, Sep. 2014.
19. D'Amore, M., M. S. Sarto, and A. G. D'Aloia, "Skin-effect modeling of carbon nanotube bundles: The high-frequency effective impedance," *2010 IEEE International Symposium on Electromagnetic Compatibility (EMC)*, 847–852, 2010, ISSN: 978-1-4244-6305-3.
20. Kadhom, M. J., J. S. Aziz, and R. S. Fyath, "Performance prediction of carbon nano tube dipole antenna using the complex permittivity approach," *Journal of Emerging Trends in Computing and Information Sciences*, Vol. 3, No. 12, 1586–1605, Dec. 2012.
21. Balanis, C. A., *Antenna Theory: Analysis and Design,* 3rd Edition, Wiley, 2005, ISBN: 0-471-66782-X.
22. Duroc, Y., "Ultra-wideband antenna arrays: Systems with transfer function and impulse response," *Progress In Electromagnetics Research M*, Vol. 34, 117–123, 2014.
23. Haupt, R. L., *Antenna Arrays: A Computational Approach,* Wiley, 2010, ISBN: 978-0-470-40775-2.